Available online at www.sciencedirect.com
ScienceDirect
Journal of the European Ceramic Society 30 (2010) 193–198
www.elsevier.com/locate/jeurceramsoc

Thermo-reversible sol–gel transition of TiO_2 nanoparticles with surface modified by p-toluene sulfonic acid

Renata C.K. Kaminski [a,b,*], Sandra H. Pulcinelli [a], Celso V. Santilli [a], Florian Meneau [b], Stéphanie Blanchandin [b], Valérie Briois [b]

[a] *Instituto de Química UNESP, Rua Professor Francisco Degni, s/n, 14800-900 Araraquara, SP, Brazil*
[b] *Synchrotron SOLEIL L'Orme des Merisiers, BP48, Saint-Aubin, 91192 Gif-sur Yvette, France*

Received 20 September 2008; accepted 19 June 2009
Available online 21 July 2009

Abstract

In this paper an unprecedent thermo-reversible sol–gel transition for titania nanoparticles dispersed in a solution of p-toluene sulfonic acid (PTSH) in isopropanol is reported. The sol formed by the thermo-hydrolysis at 60 °C of titanium tetraisopropoxide ($Ti(O^iPr)_4$) reversibly changes into a turbid gel upon cooling to room temperature. Turbidimetric measurements performed for samples containing different nominal acidity ratios (A = [PTSH]/[Ti]) have evidenced that the gel transformation temperature increases from 20 to 35 °C as the [PTSH]/[Ti] ratio increases from 0.2 to 2.0. SAXS results indicate that the thermo-reversible gelation is associated to a reversible aggregation of a monodisperse set of titania nanoparticles with average gyration radius of ≈2 nm. From the different PTSH species evidenced by Raman spectroscopy and TG/DTA of dried gels we proposed that the thermo-reversible gelation in this systems is induced by the formation of a supramolecular network, in which the protonated surface of nanoparticles is interconnected through cooperative hydrogen bonds between $–SO_3$ groups of p-toluene sulfonic acid.

Keywords: Sol–gel transition; Titanium oxide

1. Introduction

Besides the synthesis of TiO_2 nanoparticles with controlled particle size, shape, and crystal structure, the main focus of the nanofabrication technique is shifted towards the use of these nanoparticles as building blocks for the fabrication of one-, two- and three-dimensional superstructures.[1–4] One of the great challenges of this approach is the precise control of the surface properties in order to induce the spontaneous assembly of building blocks through weak inter-particle forces such as hydrogen bonding, donor–acceptor interactions, repulsive interactions and reversible ligand–metal interaction.[5,6] For example, designed organic molecules adsorbed on TiO_2 nanoparticles have directed the bi-dimensional assembly *via* the interaction between organic molecules.[1–3] There are strong evidences that preferred attachment of titania nanoparticles along the [0 0 1] direction is a consequence of the water-promoted desorption of the organic ligands from the {0 0 1} faces of the crystalline building blocks together with the dissociative adsorption of water on these crystal faces.[3] This finding has inspired us to design more sophisticated nanoparticle surfaces, with interfacial properties capable of undergoing reversible changes according to the external conditions or stimuli.

A well-known family of soft material presenting stimuli responsive self-association is the thermo-reversible gel. In these systems the self-association between the network building blocks occurs from cooperative van der Walls or hydrogen bonds induced by changes in solvent quality (in the sense of the Flory's classification).[7,8] Although natural and synthetic polymeric thermo-reversible gels were successfully employed in the elaboration of different kinds of actuator including pulsated drug release,[8] only a few groups have reported their use to prepare patterned inorganic materials.[9] Moreover, only a few published works have documented the synthesis of inorganic systems presenting a thermo-reversible sol–gel transition, it deals with aluminum polyphosphate[10] and basic zirconium sulfate.[11,12] The thermo-reversible sol–gel transition

* Corresponding author at: Instituto de Química UNESP, Rua Professor Francisco Degni, s/n, 14800-900 Araraquara, SP, Brazil.
E-mail address: renata.kaminski@synchrotron-soleil.fr (R.C.K. Kaminski).

0955-2219/$ – see front matter © 2009 Elsevier Ltd. All rights reserved.
doi:10.1016/j.jeurceramsoc.2009.06.031

of basic zirconium sulfate building blocks in water solution is governed by the temperature-dependent ionic adsorption and ionic exchange capacities involving both Cl^- and SO_4^{2-} anions.[12] Recently some of us have demonstrated the possibility to combine this thermo-reversible sol–gel system with hexagonal swollen liquid crystals or oil/water emulsion to synthesize platelet-like particles or macroscopic fibers of zirconia showing hierarchical nanoscopic structure.[13,14] Furthermore, the production of hierarchical ceramic foam by combining this thermo-induced sol–gel transition to a dual templating process of pores by oil drops and gas bubbles was recently reported.[15]

This paper is a result of our continuous effort to develop new surface modified inorganic nanoparticles presenting a thermo-induced sol–gel transition. Herein we provide evidences for the thermo-reversible behaviour of alcohol sol formed by the surface modification of TiO_2 nanoparticles with p-toluene sulfonic acid (PTSH). Aiming to understand this striking thermo-stimulated phenomenon, the effect of the molar acidity ratio ($A = [PTSH]/[Ti]$) on the thermo-reversible sol–gel transition was evaluated by small angle X-ray scattering (SAXS) and turbidity measurements carried out *in situ* during thermal cycles. The structural modification occurring in the bulk and on the surface of inorganic building blocks was elucidated by SAXS, X-ray powder diffraction (XRPD), Raman spectroscopy, thermo-gravimetric (TG) and differential thermo-analysis (DTA) measurements carried out for dried powders.

2. Experimental

TiO_2 nanoparticles were prepared by drop by drop addition of a PTSH aqueous solution to a solution of titanium tetraisopropoxide ($Ti(O^iPr)_4$) in isopropanol maintained under magnetic stirring at room temperature. The clear solution was placed in a reflux apparatus at 60 °C for 18 h fitted with a condenser and a $CaCl_2$ trap to avoid moisture exposure during the thermo-hydrolysis. The hydrolysis ratio, $H = [H_2O]/[Ti]$, was fixed at 2.3 and the acidity ratio, $A = [PTSH]/[Ti]$ was varied between 0.05 and 2. We have noted that transparent sol is transformed into a turbid gel during cooling to room temperature. Powdered xerogels were obtained after drying in an oven at 100 °C during 24 h.

The thermo-reversibility of this system was monitored *in situ* by turbidity measurements carried out during several thermal cycles between 5 and 60 °C at a controlled rate (±0.5 °C min^{-1}). Data collection was carried out in a HATCH 2100 turbidimeter using a tungsten polychromatic light and equipped with a special thermostated cell.

The SAXS experiments on the dried powders have been carried out at the SWING beam line of the French Synchrotron Radiation Source (SOLEIL). SAXS measurements were recorded with the AVIEX (Fast-Readout, Low Noise) CCD camera, placed in a vacuum detection tunnel. The sample to detector distance was fixed at 2.5 m and a beam stop of 3 mm (vertical size) with a photodiode inserted in its centre enabled to measure the transmitted intensity. This set-up allows a scattering vector, q, range between 0.033 and 3.5 nm^{-1}. The SAXS measurements of sol and gel were performed on the SAXS beamline of LNLS (Campinas, Brazil) according to the previously detailed procedure.[16]

The crystalline phases were analysed by XRPD with a Siemens D5000 diffractometer, using the Cu Kα radiation selected by a curved graphite monochromator. Simultaneous thermo-gravimetric (TG) and differential thermo-analysis (DTA) of dried powders were measured from room temperature to 850 °C under oxygen flux and heating rate of 10 °C min^{-1}, by using a SDT2960 (TA Instruments) apparatus. Raman spectra of dried powders were acquired using a Kaiser RXN1 spectrometer equipped with a 785 nm laser diode. Spectra were obtained at 20 mW of power at the sample within the 100–3200 cm^{-1} range, 100 frames accumulated, 10 s for each frame.

3. Results and discussion

The thermo-reversible sol–gel transition is evidenced by the evolution of the turbidity during the thermal cycle shown in Fig. 1, in which the liquefaction during heating is characterized by an abrupt decrease in light scattering above the gel–sol transition temperature, T_s. During cooling, the original turbidity is recovered below the sol–gel transition temperature T_g. As T_g is always lower than T_s, this phenomenon is characterized by an hysteresis loop. As illustrated by the comparison of behaviours of samples prepared with $A = 0.2$ and 2.0, the increase of the acidity radio, A, leads to a continuous increase of both transition temperatures, T_g and T_s, and of the area of the hysteresis loop. It is noteworthy that transparent and thermo-stable sol was produced for $A \leq 0.15$. This finding indicates that the interaction between the building blocks of the gel framework is promoted by PTSH species.

Relevant information about the nanostructural features of thermo-reversible sample prepared with $A = 0.35$ was revealed by SAXS measurements done in the gel (60 °C) and in the sol (5 °C) states and in the extracted dried powder (Fig. 2). Two regions can be distinguished in the log–log plot of SAXS intensity $I(q)$ curve corresponding to the sol characterized by:

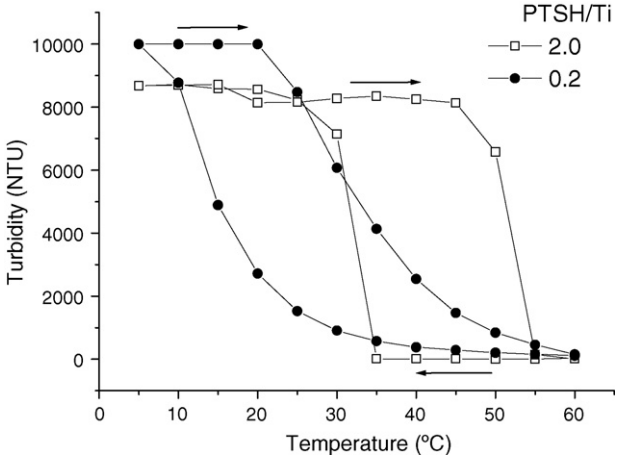

Fig. 1. Turbidity evolution as a function of the temperature during a thermal cycle for samples with [PTSH]/[Ti] = 0.2 (full symbols) and 2 (open symbols). The arrows indicate the sense of temperature modification during the thermal cycle.

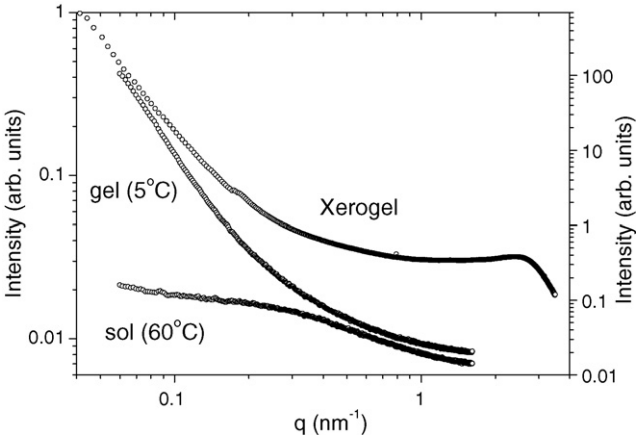

Fig. 2. SAXS curves for sol, gel and dried xerogel obtained with [PTSH]/[Ti] = 0.35. The curves are vertically shifted for sake of clarity.

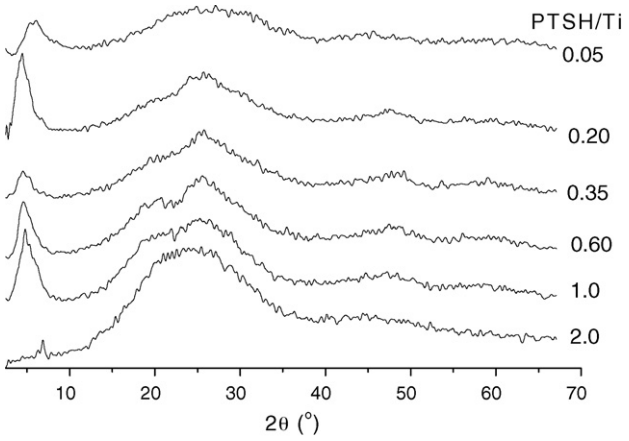

Fig. 3. XRPD patterns of dried powders prepared with different acidity ratios. The patterns are vertically shifted for sake of clarity.

(i) an essentially invariant intensity at small q ($q < 0.2\,nm^{-1}$) and (ii) an increase in the modulus of the slope at high q values ($q > 0.3\,nm^{-1}$), which is the beginning of the Porod regime ($I(q) \propto q^{-4}$).[17] This feature indicates the existence of a monodisperse set of small nanometric particles without detectable spatial correlation. An average gyration radius of about 2 nm was calculated from the Guinier law[17] for the particles detected in the sol. The single linear decay regime observed in the low q-range of curve recorded in the gel state presents a slope of −2.2, suggesting the formation of aggregates with a fractal structure. A number of experimental and computer simulation studies demonstrate that the fractal dimensionality (D_f) of 2.1 conjugated with a fast gelation process is characteristic of cluster–cluster aggregate growth limited by diffusion.[18] Thus it seems consistent to attribute this thermo-reversible sol–gel phenomenon to the diffusion-limited reversible aggregation of the primary particles present in the hot sol.

The main feature of the SAXS curve corresponding to the dried gel is the ill-defined maximum, similar to that observed in previous studies of concentrated TiO_2 sol and fired TiO_2 films.[16] This peak was attributed to interference effects in the X-ray scattering amplitude arising from spatial correlation of particles and pores in the powdered xerogel.[16] In the low q region ($q < 0.15\,nm^{-1}$), the intensity increases for decreasing q, indicating the presence of a coarser structural level. The nanostructural parameter of this multiple level structure was determined by using a semi-empirical equation proposed by Beaucage which takes into account the Guinier and Porod asymptotic trends and the correlation effects.[17] Taking into account for the hard sphere interference correlation effect only, we have find that the scattering object composing the fine structural level has an average gyration radius of about 1.0 nm with a correlation distance (ξ) of 2.2 nm and a packing factor of 1.5. This packing factor value is much lower than the one expected for the closest packing of spheres ($k = 5.92$).[17] It is important to note that this average gyration radius is about a half the Rg values of primary particles in the sol. This suggests that the fine scatters probed by SAXS in the powder are the pores formed by primary particle array. The ill-defined maximum can be explained by the weak degree of correlation revealed by the low value of the packing factor and also by the low electronic density contrast between the pores filled with organics like PTSH. This assumption is supported by the absence of the open pores and the irrelevant specific surface area value ($1.5\,m^2\,g^{-1}$) measured by N_2 adsorption isotherms. Furthermore, as the contribution at low q region ($q < 0.15\,nm^{-1}$) is similar to that observed for the gel state SAXS curve, we have attributed this coarse nanostructural level of xerogel to the hierarchical structure resulting from the aggregation process.

Fig. 3 compares the XRPD patterns of powdered xerogels derived from samples prepared with different acidity ratios. All XRPD patterns show a broad peak centred at the position of the mean diffraction plane (1 0 1) of the nanocrystalline anatase and a low angle shoulder that does not correspond to a known titanium oxide crystalline phase. Both contributions were deconvoluted by using two pseudo-Voigt functions in order to evaluate the average crystallite size (D) of anatase phase. Assuming that the peak broadening of the deconvoluted [1 0 1] anatase peak is essentially due to size effects, the value of average crystallite size calculated from the Scherrer relation was essentially invariant with the acidity ratio ($D \approx 0.8$ nm). Furthermore, it is apparent at low angle region ($2\theta < 8°$) a well-defined peak with a Bragg distance equal to the value of the correlation distance (ξ) calculated from the ill-defined peak observed in the SAXS curve of the corresponding powder. Accordingly, we have attributed this diffraction peak to the spatially correlated voids present between particles. As shown in column 2 of Table 1 the ξ value abruptly increases from 1.5 to 2.0 nm as the acidity ratio increases from 0.05 to 0.2. Since the average crystallite size remains essentially invariant, this finding indicates the effective occupation of the inter-nanoparticles space by the PTSH molecules. On opposition a decreasing trend of ξ is observed as the A value increases from 0.2 to 2 suggesting the formation of a more compact packing of nanoparticles.

The relative mass loss (TG) and differential thermal analysis (DTA) curves corresponding to dried powders prepared with different acidity ratios are presented in Fig. 4. The mass loss (15–27%) observed for temperatures lower than 150 °C can be

Table 1
Effect of the PTSH/Ti ratio on the correlation distance, experimental and nominal PTSH mass loss and ratio between the intensity of the Raman band at 1127 (υ_1(SO) of SO_3H) and at 801 cm^{-1} (υ(C–S)), $I^{SO}3^{H}/I^{CS}$.

PTSH/Ti	Correlation distance, ξ (nm)	TG mass loss between 350 and 850 °C (%)	Nominal PTSH mass loss (%)	$I^{SO}3^{H}/I^{CS}$
0.05	1.47	18.5	10.6	–
0.20	1.96	40.1	32.3	1.46
0.35	1.88	45.6	45.5	1.45
0.60	1.83	55.8	58.8	1.30
1.0	1.75	71.3	70.4	1.37
2.0	1.30	85.0	82.7	1.27

attributed to desorption of water and organic species. A striking increase of the relative mass loss above 330 °C is observed when the nominal PTSH loading increases, allowing to ascribe this event to the degradation of PTSH. However, for the powders prepared with $A > 0.6$, this mass loss occurs in two well resolved steps: the first one, between 330 and 400 °C with a mass loss of ≈10–12% is accompanied by a weak exothermic peak, whereas the second one shows a more intense exothermic mass loss between 420 and 520 °C. The presence of two exothermic peaks in samples prepared with $A = 0.35$ and 0.6 suggests that this double decomposition step occurs also for these samples in spite of the less resolved TG pattern. Finally, for samples with $A \leq 0.2$, a third exothermic peak centred at 525–540 °C is evidenced on the DTA curves. In order to have some insights concerning the origin of these thermo-decomposition steps, Table 1 compares the value of relative weight mass loss observed above 330 °C (column 3) with the value expected from the nominal amount of PTSH used in the synthesis (column 4) of the different samples. The good agreement between the nominal and experimental weight loss verified for $A \geq 0.35$ is a strong evidence of the presence of several PTSH species. Namely, as the decomposition of solid PTSH is completed at 350 °C, we ascribe the first low temperature step to the decomposition of non-dissociated PTSH species, as encountered in the solid PTSH, whereas the high temperature step is tentatively assigned to the release of surface bonded PTSH molecules. On opposition, for samples prepared with $A \leq 0.2$ the experimental weight loss is larger than that expected from the nominal amount (Table 1), evidencing the participation of another organic groups in this thermo-decomposition process, probably associated to the third exothermic peak between 510 and 580 °C.

In order to better understand the chemical nature of species involved in the thermal decomposition steps of samples prepared with different acidity ratios, the dried powders were analysed by Raman spectroscopy and compared in Fig. 5 with the spectra of PTSH and of a synthesized $[Ti_{12}O_{16}](O^{i}Pr)_{16}$ oligomeric species,[19] labelled DOTi. Band assignments reported in Fig. 5 are done according to references.[20,21] For comparison purpose, the Raman spectra of dried powders were normalized on the band at ≈1600 cm^{-1} assigned to the C–CH stretching mode in

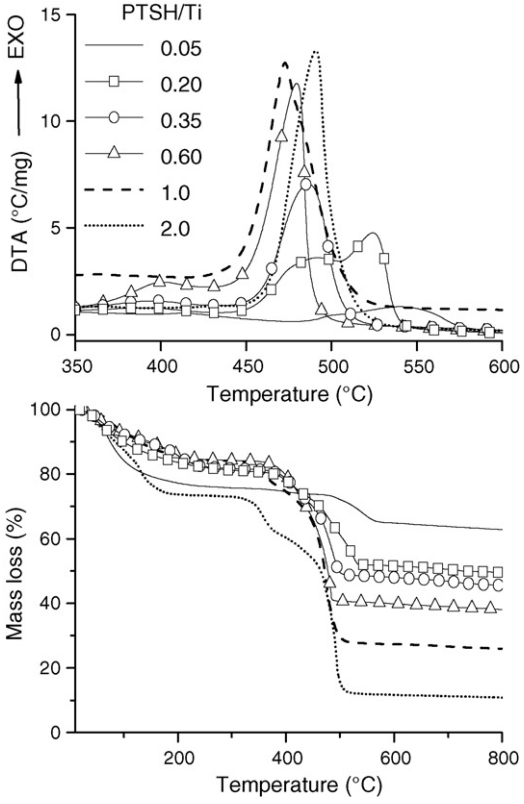

Fig. 4. DTA (a) and TG (b) curves of dried powders prepared with different [PTSH]/[Ti] ratios.

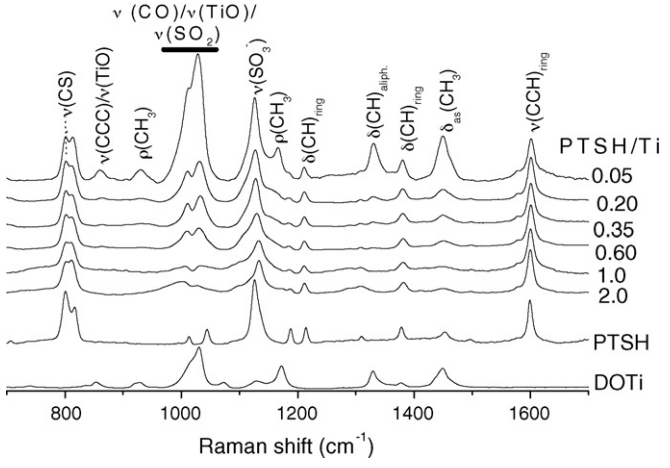

Fig. 5. Raman spectra of dried powders prepared with different [PTSH]/[Ti] ratios, p-toluene sulfonic acid (PTSH) and $[Ti_{12}O_{16}](O^{i}Pr)_{16}$ oligomeric species. (DOTi) in the 700–1700 cm^{-1} region. For comparison purpose, the spectral feature at 1600 cm^{-1} was normalized in both the dried powders and the PTSH spectra.

the PTSH aromatic ring[20]. All samples display the characteristic bands of solid PTSH, but also for some of them, several additional bands at about 1330, 1165, 930 and 855 cm^{-1} are clearly observed with decreasing intensity when the acidity ratios increase. These bands could be tentatively attributed to the vibration modes of CH, CH_3, CCC aliphatic groups and Ti–O[20]. Actually their positions are in good agreement with the bands observed for the DOTi reference suggesting, that primary particles in the powders with $A \leq 0.6$ are similar to $[Ti_{12}O_{16}](O^iPr)_{16}$ oligomeric species, and for which nuclearity should agree with the average gyration radius of particles (≈2 nm) determined by SAXS. It is important to note that in such oligomeric species[19], isopropoxyl groups are located at the periphery of the $[Ti_{12}O_{16}]$ cluster. For powders with $A \geq 1$ the bands attributed to the vibrations characteristic of the O^iPr groups of titanium oxo-oligomers totally disappear. Furthermore, it is noteworthy that except for the spectrum of the sample with $A = 0.05$, the relative intensities of the bands related to the titanium oxo-oligomer core are very small compared to the bands characteristic of groups belonging to the PTSH moiety. This allowed us to consider that the spectra for samples with $A \geq 0.2$ are mainly dominated by the vibrations of the PTSH moiety. As a consequence the bands at ≈1127–1133 and 1033–1028 cm^{-1} observed for samples with $A \geq 0.2$ can be unambiguously assigned to υ_1(SO) modes of undissociated sulfonic acid and sulfonate groups, respectively, indicating that the xerogel contains both $–SO_3H$ and $–SO_3^-$ ligands. According to Edwards and Smith[22] the degree of association of the p-toluene sulfonic acid is proportional to the ratio of the normalized intensity of the band at 1127 cm^{-1}, related to the concentration of the unionized PTSH species (SO_3H), over the normalized intensity of the υ (C–S) band at 801 cm^{-1}, related to the total acid concentration. As shown in Table 1 the values of $I^{SO}3^H/I^{CS}$ present a decreasing trend as the acidity ratio increases, indicating that the SO_3H association degree slowly decreases giving rise to the formation of more sulfonated species. Taking into account the chemical species revealed by Raman we have assigned the double decomposition step observed in TG/DTA curves to the release of unionized and ionized PTSH molecules, occurring for $A \geq 0.6$ between 330–400 and 420–515 °C, respectively. Moreover, the exothermic weight loss verified above 520 °C in the sample prepared with $A = 0.2$ and 0.05 is assigned to the release of $–O^iPr$ decomposition products.

Face to the experimental results, the role of the PTSH proportion on the formation of TiO_2-based nanoparticles presenting thermo-reversible sol–gel transition can be explained as follows. The thermo-hydrolysis of titanium isopropoxide at 60 °C in the presence of PTSH and $[H_2O]/[Ti] = 2.3$ gives rise to the formation of titanium oxo-oligomers (nanoparticles) with an average gyration radius of about 2 nm. At low acidity ratio ($A = 0.05$), these nanoparticles are not aggregated in the sol state because they are surface capped with isopropoxyl groups (O^iPr). The presence of this surface ligand, revealed by thermo-gravimetric analysis and suggested by the analogy with the Raman spectra of the DOTi, prevents the particles aggregation leading to a thermo-stable sol. Upon the increase of the acidity ratio, hydrolysis of surface bonded isopropoxyl groups occurs favouring the exchange of the capping ligand and the efficient protonation of the titania nanoparticle surface. As a consequence the ionic interaction between the $–SO_3^-$ groups of ionized PTSH and the positively charged surface of nanoparticles may occur. The existence of unionized and ionized PTSH species in the solid state, revealed by Ramam spectroscopy and TG/DTA data, suggests that these species are in equilibrium in both the sol and the gel state. As a consequence, the formation of different hydrogen bonding structures is expected to be a function of temperature, chemical composition of nanoparticle surface, PTSH/Ti and $PTSH/H_2O$ ratios.

The thermo-reversible behaviour here described for the TiO_2 nanoparticles in the presence of PTSH is qualitatively similar to that observed in some polymer solutions with an upper critical solution temperature (UCST), in which phase separation and gelation occur below a critical temperature.[7,8] In biological thermo-reversible gels, this behaviour is often assigned to cooperative hydrogen bonding between macromolecules that enjoy lifetimes longer than in water–water associations.[8] The cooperative effect is reflected by the lowering of the barrier energy for hydrogen bond formation when the neighbouring group has been hydrogen bonded. Due to the sharp decrease of the lifetimes of hydrogen bonds with the increase of the temperature the gel liquefies upon heating.[8] The aggregation of sulfonic acid groups through cooperative hydrogen bonding and their key role in the swelling of polymeric resins gel have already been identified.[20] Thus, it seems consistent to attribute the thermo-reversible gel formation described in this paper to the formation of a supramolecular network in which the protonated surfaces of nanoparticles are interconnected through cooperative hydrogen bonding between $–SO_3H$ groups of undissociated p-toluene sulfonic acid, water molecules and ionized species ($–TiOH^+$, $–SO_3^-$).

4. Conclusions

Using a one-pot sol–gel synthesis, titania nanoparticles were obtained as thermo-reversible sol presenting an upper critical solution temperature (UCST), in which gelation occurs below a critical temperature. This unprecedent behaviour within inorganic systems is due to the formation of a supramolecular network in which the ionized species present at the surface of the protonated titanium nanoparticles are interconnected through cooperative hydrogen bonding between $–SO_3H$ groups of p-toluene sulfonic acid. The critical gelation temperature in this system can be finely tuned between 20 and 35 °C by increasing the [PTSH]/[Ti] ratio from 0.2 to 2, when $[H_2O]/[Ti]$ is equal to 2.3.

Although the results here presented are only based on titania nanoparticles in the presence of p-toluene sulfonic acid in isopropanol solution, it should be possible to extend this thermo-reversible sol–gel concept to other inorganic systems. The fast gelation observed upon cooling can be exploited setting gas bubbles or oil drops for the production of ceramic foams. Furthermore, the compact packing of TiO_2 nanoparticles regularly spaced by the PTSH capping layer as reported for the dried gel may be useful in the preparation of high quality thin films.

Acknowledgements

The authors thank the collaboration of LNLS and SOLEIL staff during the SAXS measurements and the financial support from CAPES/COFECUB, CNPQ and FAPESP.

References

1. Cozzoli, P. D., Kornowski, A. and Weller, H., Low-temperature synthesis of soluble and processable organic-capped anatase TiO_2 nanorods. *J. Am. Chem. Soc.*, 2003, **125**, 14539–14548.
2. Jun, Y. W., Casula, M. F., Sim, J. H., Kim, S. Y., Cheon, J. and Alivisatos, A. P., Surfactant-assisted elimination of a high energy facet as a means of controlling the shapes of TiO_2 nanocrystals. *J. Am. Chem. Soc.*, 2003, **125**, 15981–15985.
3. Polleux, J., Pinna, N., Antonietti, M., Hess, C., Wild, U., Schlögl, R. *et al.*, Ligand functionality as a versatile tool to control the assembly behavior of preformed titania nanocrystals. *Chem. Eur. J.*, 2005, **11**, 3541–3551.
4. Sakatani, Y., Boissière, C., Grosso, D., Nicole, L., Soler-Illia, G. J. A. and Sanchez, A. C., Coupling nanobuilding block and breath figures approaches for the designed construction of hierarchically templated porous materials and membranes. *Chem. Mater.*, 2008, **20**, 1049–1056.
5. Colfen, H. and Mann, S., Higher-ordered organization by mesoscale self-assembly and transformation of hybrid nanostructures. *Angew. Chem. Int. Ed.*, 2003, **42**, 2350–2365.
6. Oaki, Y., Kotachi, A., Miura, T. and Imai, H., Bridged nanocrystals in biominerals and their biomimetics: classical yet modern crystal growth on the nanoscale. *Adv. Funct. Mater.*, 2006, **16**, 1633–1639.
7. Guenet, J. M., *Thermoreversible Gelation of Polymers and Biopolymers*. Academic Press, London, 1992 [Chapter 1].
8. Bromberg, L. E. and Ron, E. S., Temperature-responsive gels and thermogelling polymer matrices for protein and peptide delivery. *Adv. Drug Deliv. Rev.*, 1998, **31**, 197–221.
9. Wang, H., Holmberg, B. and Yan, Y., Synthesis of template-free zeolite nanocrystals by using in situ thermoreversible polymer hydrogels. *J. Am. Chem. Soc.*, 2003, **125**, 9928–9929.
10. Lima, E. C. O. and Galembeck, F., Thermorevesible gel formation from aqueous aluminum polyphosphate solutions. *J. Colloid Interf. Sci.*, 1994, **166**, 309–315.
11. Chiavacci, L. A., Pulcinelli, S. H., Santilli, C. V. and Briois, V., Structural and phenomenological characterization of the thermoreversible sol–gel transition of a zirconyl aqueous precursor modified by sulfuric acid. *Chem. Mater.*, 1998, **10**, 986–993.
12. Chiavacci, L. A., Santilli, C. V., Pulcinelli, S. H., Bourgaux, C. and Briois, V., Role of the surface state and structural feature in the thermoreversible sol–gel transition of a zirconyl aqueous precursor modified by sulfuric acid. *Chem. Mater.*, 2004, **16**, 3995–4004.
13. Santos, E. P., Santilli, C. V., Pulcinelli, S. H. and Prouzet, E., Zirconia needles synthesized inside hexagonal swollen liquid crystals. *Chem. Mater.*, 2004, **16**, 4187–4192.
14. Alves Rosa, M. A., Sanhueza, C. S. S., Santilli, C. V., Pulcinelli, S. H. and Briois, V., Stimuli-responsive controlled growth of mono- and bidimensional particles from basic zirconium sulfate hydrosols. *J. Phys. Chem. B*, 2008, **112**, 9006–9012.
15. Alves Rosa, M. A., Santos, E. P., Santilli, C. V. and Pulcinelli, S. H., Zirconia foams prepared by integration of the sol–gel method and dual soft template techniques. *J. Non-Cryst. Solids*, 2008, **354**, 4786–4789.
16. Kaminski, R. C., Pulcinelli, S. H., Craievich, A. F. and Santilli, C. V., Nanocrystalline anatase thin films prepared from redispersible sol–gel powders. *J. Eur. Ceram. Soc.*, 2005, **25**, 2175–2180.
17. Craievich, A. F., Small-angle X-ray scattering by nanostructured materials. In *Handbook of Sol–Gel Science and Technology*, *vol. II*, ed. R. M. Almeida. Kluwer Academic Publishers, Boston, 2004, pp. 159–190.
18. Brinker, C. J. and Scherer, G. W., *Sol–Gel Science: The Physics and Chemistry of Sol–Gel Processing*. Academic Press, San Diego, 1990 [Chapter 5].
19. Day, V. W., Eberspacher, T. A., Klemperer, W. G. and Park, C. W., Dodecatitanates: a new family of stable polyoxotitanates. *J. Am. Chem. Soc.*, 1993, **115**, 8469–8470.
20. Edwards, H. G. M., Brown, D. R., Dale, J. R. and Plant, S., Raman spectroscopic studies of acid dissociation in sulfonated polystyrene resins. *J. Mol. Struct.*, 2001, **595**, 111–125.
21. Moran, P. D., Bowmaker, G. A., Cooney, R. P., Finnie, K. S., Bartlett, J. R. and Woolfrey, J. L., Vibrational spectra and molecular association of titanium tetraisopropoxyde. *Inorg. Chem.*, 1998, **37**, 2741–2748.
22. Edwards, H. G. and Smith, D. N., The Raman spectrum of ethanesulphonic acid, $C_2H_5SO_3H$, and the ethanesulfonate ion. *J. Mol. Struct.*, 1990, **238**, 27–41.